Biosensors and Bioelectronics 276 (2025) 117256

Contents lists available at ScienceDirect

Biosensors and Bioelectronics

journal homepage: www.elsevier.com/locate/bios

Droplet pairing-merging enabled digital RPA-CRISPR/Cas12a (DIMERIC) assay for rapid and precise quantification of Hepatitis B Virus DNA

Dongyang Cai [a,b,1], Yifan Wang [a,1], Ziyi Zhang [c,1], Enqi Huang [a], Na Yang [a], Xiao Yang [a], Ting Zhang [a], Hongting Wen [a], Yu Wang [a,d], Zhenhua Chen [a], Hongkai Wu [e], Dayu Liu [a,b,*]

[a] Department of Laboratory Medicine, The Second Affiliated Hospital, School of Medicine, South China University of Technology, Guangzhou, 510180, China
[b] Guangdong Engineering Technology Research Center of Microfluidic Chip Medical Diagnosis, Guangzhou, 510180, China
[c] Department of Urology, The Second Affiliated Hospital, Dalian Medical University, Dalian, 116021, China
[d] Micro-Nano Tech Center, Bioland Laboratory, Guangzhou, 510005, China
[e] Department of Chemistry, Hong Kong University of Science and Technology, Hong Kong, China

ARTICLE INFO

Keywords:
Microfluidics
Droplet pairing-merging
Digital assay
RPA-CRISPR/Cas12a
Hepatitis B virus DNA

ABSTRACT

Recombinase polymerase amplification (RPA)-CRISPR/Cas12a assays have demonstrated remarkable potential for point-of-care detection of pathogens in resource-limited settings. Nevertheless, these assays fall short in delivering direct quantitative results due to the incompatibility between the RPA and CRISPR/Cas12a systems. To overcome this limitation, we developed a droplet pairing-merging enabled digital RPA-CRISPR/Cas12a (DIMERIC) assay in this study. By leveraging a microfluidic chip with a calabash-shaped microwell array, large-volume RPA droplets and small-volume CRISPR/Cas12a droplets were sequentially and size-selectively trapped, generating one-to-one droplet pairs. This spatial separation of the droplets eliminates the inhibitory effects of the CRISPR/Cas12a chemistry on RPA. Upon the completion of RPA, the CRISPR/Cas12a system can be activated by merging the paired droplets. This temporal separation of the RPA and CRISPR/Cas reactions allows for the accumulation of sufficient amplicons to efficiently unleash the collateral cleavage activity. The DIMERIC assay offers rapid quantification of nucleic acids, with the entire procedure being accomplished within 20 min. This assay was employed for the quantitative detection of Hepatitis B virus DNA from batched clinical serum samples, demonstrating a good correlation with qPCR (R^2 = 0.92033) and ddPCR (R^2 = 0.97337) outcomes. Consequently, the developed DIMERIC assay provides a valuable tool for rapid and precise quantification of pathogenic nucleic acids.

1. Introduction

Clustered regularly interspaced short palindromic repeats-CRISPR associated (CRISPR-Cas) systems play a crucial role in the microbial adaptive immune system that uses CRISPR RNA (crRNA)-guided nucleases to degrade invading nucleic acids (Barrangou et al., 2007; Marraffini and Sontheimer, 2008). To date, the CRISPR-Cas systems have been used in a wide range of biomedical applications, including gene editing, nucleic acid imaging, and cellular event recording (Chen et al., 2013; Cong et al., 2013; Sheth et al., 2017). Recently, CRISPR-based diagnostics (CRISPR-Dx) have attracted increasing attention due to their remarkable specificity, programmability, and ease of use (Kaminski et al., 2021). Upon target recognition by crRNA, the activated Cas nucleases unleash collateral activity to cleave non-target single-stranded (ss) DNA/RNA reporter molecules, releasing the caged fluorophores that can be detected with lateral-flow and fluorescence readouts (Gootenberg et al., 2018). By integrating with an isothermal nucleic acid amplification (INA) step, ultrasensitive assays such as SHERLOCK and DETECTR (with attomolar sensitivity) have been developed (Chen et al., 2018; Gootenberg et al., 2017). To streamline the testing procedures and minimize the risk of carryover contamination inherent in these two-step methods, several one-pot assays such as STOPCovid, SHINE, sPAMC, AIOD-CRISPR, and HOLMESv2 have been developed subsequently (Arizti-Sanz et al., 2020; Ding et al., 2020;

* Corresponding author. Department of Laboratory Medicine, the Second Affiliated Hospital, School of Medicine, South China University of Technology, Guangzhou, 510180, China.
E-mail address: eydyliu@scut.edu.cn (D. Liu).
[1] These authors contribute equally to the study.

https://doi.org/10.1016/j.bios.2025.117256
Received 16 December 2024; Received in revised form 11 February 2025; Accepted 11 February 2025
Available online 12 February 2025
0956-5663/© 2025 Elsevier B.V. All rights are reserved, including those for text and data mining, AI training, and similar technologies.

Joung et al., 2020; Li et al., 2019; Lu et al., 2022). Nevertheless, both the two-step and one-pot CRISPR methods were primarily designed for qualitative detection rather than quantification. In the two-step methods, rapid reaction saturation during the initial INA step impedes the acquisition of quantitative results (i.e., different amounts of template yield similar end-point fluorescence signals) (Gootenberg et al., 2017). Conversely, in the one-pot methods, where target amplification occurs concurrently with collateral cleavage, extensive optimization is necessary to balance the dynamic reactions and eliminate their mutual interference; otherwise, low detection sensitivity will result (Yao et al., 2024). Additionally, real-time monitoring of fluorescence signals (like qPCR) is required for precise nucleic acid quantification (Kaminski et al., 2021). Since quantitative detection of pathogenic nucleic acids is essential for the diagnosis of infectious diseases, either for assessing disease stage or for determining treatment plan, the advancement of the quantification capabilities of CRISPR-Dx holds substantial practical significance.

To achieve precise nucleic acid quantification, several studies have recently reported digital CRISPR assays, such as deCOViD, RADICA, MEDICA, PADLOCK, DropCRISPR, CASMART, and dWS-CRISPR (Cui et al., 2022; Ding et al., 2021; Liu et al., 2022; Park et al., 2021; Wu et al. 2021, 2022; Zhang et al., 2023). Following the concept of digital detection, these digital CRISPR assays realized absolute quantification by confining a single target within numerous compartments and then performing Poisson statistical analysis of the end-point binary readouts from each compartment. The digital quantification format obviates the dependence on standard curves, meanwhile the end-point detection format eliminates the need for complex optical setups. Unlike digital PCR, which depends on precise temperature control apparatuses, digital CRISPR assays can be implemented under isothermal conditions. Additionally, integrating CRISPR detection with digital INA (e.g., RPA and LAMP) can prevent false-positive results caused by inherent non-specific amplification. Consequently, digital CRISPR assays are suitable for pathogenic nucleic acid quantification.

Despite the significant progress achieved in digital CRISPR assays, several challenges remain to be addressed for their successful application in clinical diagnostics. One of the major challenges is the incompatibility between INA and the CRISPR system. For instance, in the widely used RPA-CRISPR/Cas12a system, the Cas12a nuclease continuously degrades RPA templates and amplicons through cis cleavage and RPA primers through trans cleavage, resulting in reduced detection sensitivity and delayed detection time (Li et al., 2019; Wang et al., 2019). This undesired cleavage is particularly problematic in digital CRISPR assays, where each compartment contains a limited number of target molecules, thereby increasing the likelihood of false-negative results. In bulk-volume CRISPR assays, this issue was addressed by spatial or phase separation of the INA and CRISPR/Cas systems. Specifically, the CRISPR reagents were applied to the lid or wall of the tube (Hu et al., 2022a; Wang et al., 2019). Alternatively, the reactions were modified by incorporating substances with high density and/or viscosity, such as sucrose, glycerol, or agarose gel, into the closed system (Lin et al., 2022; Uno et al., 2023; Yin et al., 2020). There is another method that employed photochemically controlled crRNA to block the cis recognition process during the RPA reaction (Chen et al., 2022; Hu et al., 2022b). Nevertheless, these strategies are not readily applicable to the large-scale compartments used in digital CRISPR assays. One method has been effectively implemented in digital RPA-CRISPR/Cas12a, wherein protospacer adjacent motif (PAM)-free crRNAs were designed to target the ssDNA generated exclusively after RPA strand displacement (Wu et al., 2021; Xia et al., 2023). Nevertheless, this method suffers several limitations including location restrictions, unclear optimization mechanisms, and incompatibility with other INA methods (Lin et al., 2023).

Droplet microfluidics provides high flexibility in droplet manipulation, including droplet pairing and merging (Enqi Huang et al., 2024). The microfluidic chip patterned with symmetrical figure-of-eight microwells has been used to confine multiple droplets, enabling the formation of closely connected droplet pairs (Kulesa et al., 2018). This configuration allows the transfer of reagents from one droplet to another through droplet merging, thereby facilitating the execution of sequential and/or combinatorial biochemical reactions on a large scale. For instance, Ackerman et al. have developed droplet pairing-merging enabled RPA/PCR-CRISPR platforms, namely CARMEN and bCARMEN, and demonstrated their feasibility in high-throughput pathogen detection (Ackerman et al., 2020; Thakku et al., 2022). Nevertheless, a notable limitation of this method is the inevitable pairing of droplets containing identical content, leading to a considerable proportion of invalid reaction units. These artificial "negative" units, which form the foundation of Poisson statistics-based digital analysis, can result in an underestimation of target nucleic acids. To address this issue, Cai et al. and Wu et al. have independently developed a "calabash-shaped" microwell array chip. These specially configured microwells facilitated the sequential and size-selective trapping of template droplets and primer droplets from different libraries into their corresponding sub-wells (Cai et al., 2023; Wu et al., 2023). By integrating this unique chip configuration with droplet encoding strategies, they have successfully developed high-order multiplexed droplet digital INA assays.

In this study, we developed a **d**roplet pa**i**ring-**m**erging **e**nabled digital **R**PA-CR**I**SPR/**C**as12a (DIMERIC) assay. The DIMERIC assay addresses the incompatibility between RPA and CRISPR/Cas12a by deploying a droplet pairing-merging strategy. The "calabash-shaped" microwell array enables sequential and size-selective trapping of large-volume RPA droplets and small-volume CRISPR/Cas12a droplets. This configuration ensures that the RPA reaction remains unaffected by the CRISPR/Cas12a chemistry. Upon the completion of RPA, CRISPR detection was activated through merging the paired droplets. By spatially and temporally separating the RPA and CRISPR reactions, the inhibitory effects of CRISPR/Cas12a on RPA were effectively eliminated. The removal of reaction inhibition significantly reduces the time required for both RPA and CRISPR-Cas reactions, thereby shortening the total assay time of DIMERIC to 20 min. This DIMERIC assay was used to quantitatively detect Hepatitis B virus (HBV) DNA in clinical serum samples, showing a good correlation with qPCR (R^2 = 0.92033) and ddPCR (R^2 = 0.97337) outcomes. Overall, the developed DIMERIC assay provides a valuable tool for rapid and precise quantification of pathogenic nucleic acids.

2. Materials and methods

2.1. Microfluidic chip design and fabrication

RPA droplets (d = 130 μm) and CRISPR/Cas12a droplets (d = 80 μm) were generated using two distinct droplet generation chips. The RPA droplets were generated using a Y-shaped microchannel configuration, with one channel for the MgOAc initiator and another for the target-included RPA master mix. In contrast, the CRISPR/Cas12a droplets were generated using a conventional flow-focusing geometry. The "calabash-shaped" microwell array chip was designed as previously described (Cai et al., 2023). Briefly, the chip comprised a bottom layer and a top layer. The bottom layer comprised a chamber with a height of 300 μm for droplet floating, while the top layer comprised an array of "calabash-shaped" microwells (10,000 microwells) that were arranged in a lattice pattern (50 μm inter-well spacing) for droplet trapping. Each "calabash-shaped" microwell comprised two cylindrical structures: a smaller one with a diameter of 90 μm and a depth of 65 μm, and a larger one with a diameter of 135 μm and a depth of 110 μm. The small and large sub-wells had a 15 μm overlap along the upper circular base (Fig. S1).

All the microfluidic chips were fabricated using standard soft lithography techniques. Briefly, SU-8 molds were fabricated on 4-inch silicon wafers through a series of procedures, including multi-step spin-coating, baking, exposure, and pattern developing, with each

procedure tailored to achieve the desired layer thickness. Subsequently, a mixture of polydimethylsiloxane (PDMS) and curing agent (Dow Corning, Sylgard 184) in a ratio of 10:1 was prepared. The PDMS mixture was poured onto the SU-8 molds and then baked at 120 °C for 20 min to transfer the patterns onto cured PDMS layers. The PDMS layer was punched with a 1 mm-diameter puncher to form inlets/outlets and then bonded together after oxygen plasma. Finally, the chips were baked at 120 °C for 24 h to restore their hydrophobicity.

2.2. Serum samples and viral DNA extraction

Twenty-four serum samples from patients with suspected HBV infection were collected at Guangzhou First People's Hospital. The HBV DNA titer of each sample was determined by real-time PCR (ABI Prism 7500) using the Hepatitis B Test Kit (DaAngene, Guangzhou). Remnant serum samples were stored at −80 °C until analysis. Viral DNA extraction from 200 μL serum samples was performed using the Magnetic Viral DNA/RNA Kit (Tiangen Biotech., Beijing) following the manufacturer's instructions. The collection of all clinical samples received approval from the Ethics Committee of Guangzhou First People's Hospital (IRB: K-2021-057-01), and the study was conducted in compliance with ethical standards.

2.3. Chemistry of the DIMERIC assay

The MgOAc initiator phase (50 μL) comprised 1× rehydration buffer (29.5 μL), 28 mM magnesium acetate (MgOAc), and 2 μM Alexa Fluor 647 (ThermoFisher). The RPA master mix phase (50 μL) comprised 1× rehydration buffer (29.5 μL), 960 nM forward and reverse primers, one lyophilized pellet from the basic RPA kit (TwistDx Limited), 0.8 U/μL RNase inhibitor Murine (New England BioLabs), and 10 μL of HBV DNA sample.

The CRISPR/Cas12a solution comprised 1× NEBuffer r2.1 (New England BioLabs), 0.8 U/μL RNase inhibitor Murine (New England BioLabs), 5.3× (200 nM EnGen LbaCas12a (New England BioLabs), 200 nM crRNA, and 1000 nM ssDNA FQ-reporter).

2.4. Operation procedure of the DIMERIC assay

The flow rates of solutions were precisely controlled with a syringe pump (RSP01-BD, Biotaor, Jiaxing, China). For generating the large-volume RPA droplets, the flow rates of both the master mix and MgOAc initiator were maintained at 2 μL/min, while the flow rate of the oil (1864006, Bio-Rad Laboratories, Inc.) was set at 30 μL/min. The generated RPA droplets were then transferred into the microwell array chip *via* pipetting. By manually tilting the chip, the RPA droplets were allowed to float up into the large sub-wells due to buoyancy forces. Once all the large sub-wells were occupied, any excess RPA droplets were flushed out from the outlet of the chip. For generating the small-volume CRISPR/Cas12a droplets, the flow rate of the Cas12a detection mix was maintained at 5 μL/min and that of the oil was set at 12 μL/min. The generated CRISPR/Cas12a droplets were transferred into the microwell array chip and then floated up into the small sub-wells. After the expulsion of untrapped droplets, the chip was incubated on a 37 °C dry bath (DKT200-4, Miulab, Hangzhou, China) for 15 min for RPA reaction. The temperature of the dry bath was monitored with a K-type thermocouple thermometer (DT-610B, CEM, Shenzhen, China). The temperature indicated by the dry bath's built-in sensor matched closely with the temperature measured by the thermometer. Subsequently, an electric field was applied to the top surface of the chip with a lighter piezoelectric ignitor to induce droplet merging (Fig. 1). After droplet merging, the final concentrations of Cas12a, crRNA, and ssDNA FQ-reporter would be 1x according to the volume ratio. Finally, the chip was incubated for a certain period of time for Cas12a-mediated cleavage.

2.5. Digital PCR

The quantification results were compared with those obtained from the DropXpertS6, a commercial digital PCR system (Biorain Technology, Shenzhen, China). The digital PCR reaction mixture (20 μL) comprised

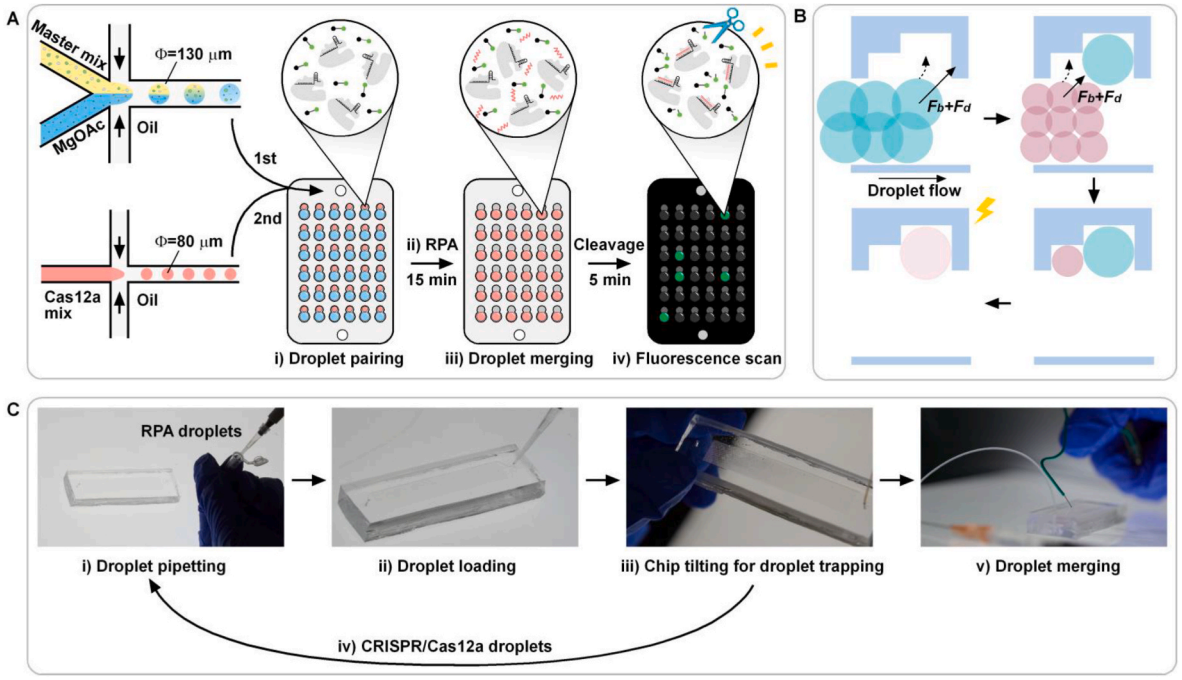


Fig. 1. Overview of the DIMERIC workflow. A) The DIMERIC workflow at the molecular and macroscopic scale. i) Droplet pairing: the RPA and CRISPR/Cas12a droplets were sequentially trapped by the calabash-shaped microwell array, forming droplet pairs; ii) RPA reaction: the chip was incubated for RPA reaction; iii) Droplet merging/CRISPR detection: after RPA reaction, the droplet pairs were merged to activate the CRISPR/Cas12a system; iv) Image fluorescence readouts: fluorescence imaging of the droplet array to count positive and negative droplets. B) Side view of the droplet trapping, pairing, and merging process. F_b represents the buoyant force of the oil and F_d represents the drag force of the oil. C) Photographs of the droplet manipulation process.

the following components: 1× AplusTM ddPCR mix (Biorain Technology), 500 nM forward and reverse primers, 500 nM Taqman probe (Table S1), 2 μL of template DNA, and 5 μL of nuclease-free water (Takara). The thermocycling conditions were as follows: 95 °C for 2 min, followed by 40 cycles of 95 °C for 20 s and 60 °C for 1 min.

2.6. Droplet array imaging

All bright-field and fluorescence images were acquired using a Leica DMi8 inverted fluorescence microscope equipped with a motorized stage and a Leica DFC7000T camera. During the imaging process, a magnification of 5× was utilized to achieve a distinct visualization of the droplets while simultaneously reducing the imaging time (~2 min). The obtained images were analyzed using imageJ software (NIH, Bethesda, MD, USA). To measure the fluorescence intensity of both positive and negative droplets, far-red fluorescence images were obtained by introducing the Alexa Fluor 647 dye (Fig. S3). Subsequently, the images were converted to 8-bit format, and the threshold option was used to delineate each droplet. By selecting appropriate size and circularity, the region of interest (ROI) of all droplets was established. Finally, the fluorescence intensity of the corresponding FAM fluorescence image was measured based on the ROI generated from the far-red fluorescence images, and a scatter plot of the fluorescence intensity was plotted (Zhang et al., 2023). The parameters for fluorescence imaging were as follows: an exposure time of 500 ms, excitation wavelengths of 475 nm and 647 nm, and emission wavelengths of 519 nm and 670 nm. All the microphotographs were stitched together using the Leica Application Suite X software.

2.7. Statistics analysis

Poisson statistics was performed with IBM SPSS Statistics software v23.0 (IBM, Armonk, NY, USA). The parameters used in the analysis included the total number of droplets counted, the number of positive droplets identified, and the volume of RPA droplets. Differences between experimental groups were evaluated by Student's t-test. P value < 0.05 was considered statistically significant.

3. Results and discussion

3.1. Droplet microfluidics enabled DIMERIC assay

We developed a digital RPA-CRISPR/Cas12a assay, termed DIMERIC, by leveraging a droplet pairing-merging strategy. The employed microfluidic chip contains a high-density microwell array that enables the formation of a substantial quantity of immobilized droplets required for digital analysis. These microwells are of a calabash shape and are designed to sequentially trap RPA and CRISPR-Cas12a droplets of different sizes. The workflow of the DIMERIC assay includes four steps (Fig. 1): i) Droplet pairing: the RPA droplets and CRISPR/Cas12a droplets were sequentially trapped by the calabash-shaped microwell array, forming one-to-one droplet pairs; ii) RPA reaction: the chip was incubated at a suitable temperature for RPA reaction. The specially configured microfluidic chip spatially separates the droplets, thereby eliminating the impact of the CRISPR/Cas12a chemistry on RPA (Fig. S2); iii) Droplet merging/CRISPR detection: when the RPA reaction was complete, the droplet pairs were merged to activate the CRISPR/Cas12a system. This temporal separation of the RPA and CRISPR/Cas reactions enables the accumulation of sufficient amplicons to efficiently unleash the collateral cleavage activity; iv) Image fluorescence readouts: fluorescence imaging of the droplet array was performed to count positive and negative droplets. By applying the Poisson statistical analysis, the number of target nucleic acids can be determined based on the proportion of positive droplets.

3.2. Generation of RPA and CRISPR/Cas12a droplets

RPA reaction initiates upon the addition of MgOAc even at room temperature (Shen et al., 2011). The premature amplification before sample partitioning can lead to an overestimation of target concentration in digital RPA (Yeh et al., 2017). To minimize this undesired amplification, it is necessary to prepare all RPA reactions on ice and promptly dispense them into miniaturized compartments, which complicates the detection procedure and requires well-trained personnel (Wu et al., 2021; Xia et al., 2023; Zhang et al., 2023). In this study, a droplet generator featuring a Y-shaped microchannel was used to combine MgOAc with the target-included RPA master mix. Upon fluid converging at the intersection of the microchannel, the reaction mixture was immediately partitioned into discrete droplets (Fig. 2A), thereby eliminating the premature amplification (Choi et al., 2023; Liu et al., 2022).

The implementation of the DIMERIC assay necessitates the formation of RPA and CRISPR/Cas12a droplet pairs. Accordingly, generating monodispersed RPA and CRISPR/Cas12a droplets of designated sizes is crucial for the size-selective trapping. The size distribution of the RPA and CRISPR/Cas12a droplets is shown in Fig. 2B. The average diameters of the RPA droplets and CRISPR/Cas12a droplets were 129.8 μm with a coefficient of variation (CV) of 1.83% and 80.1 μm with a CV of 1.72%, respectively ($n = 300$). Such uniformity in droplet size demonstrates excellent controllability of droplet generation, enabling the subsequent droplet pairing and merging process as well as collateral cleavage to proceed with high efficiency.

3.3. Droplet pairing and merging

The calabash-shaped microwell array chip enables size-selective trapping of free droplets through the combination of drag and buoyant forces of the oil phase. This design allows for the visualization of each stage in droplet manipulation. Fig. 2C, D illustrate the trapping of large-volume droplets containing yellow food dyes and small-volume droplets containing blue food dyes and thus forming one-to-one droplet pairs. Occasionally coalescent large-volume droplets (>160 μm in diameter) or small-volume droplets (>100 μm in diameter) during droplet manipulation cannot be trapped by the corresponding sub-wells. The efficiencies for droplet trapping and pairing were quantitatively assessed by analyzing the occupancy of the sub-wells. The efficiencies for trapping large-volume droplets and small-volume droplets were determined to be 99.5% and 98.6%, respectively, and that for productive droplet pairing (large-volume droplets + small-volume droplets) was 98.1% (Fig. 2F). Merging of the paired droplets was achieved with an electrical field supplied by a piezoelectric ignitor in a lighter (Fig. 2E). After merging, the 5.3× component concentrations in the CRISPR/Cas12a droplets would become 1×, thereby rendering them suitable for the CRISPR reaction. The merging efficiency on the basis of droplet pairing was determined to be 98.6% (Fig. 2F). Such high pairing and merging efficiencies ensure that the effective droplet number for target detection can be increased by simply expanding the array size. Importantly, no undesired droplet merging was observed during the RPA reaction, which could otherwise result in false-negative results.

3.4. Optimization of the DIMERIC assay

To enhance the quantification performance, we optimized several key components and reaction conditions of the DIMERIC assay. The fluorescence signal of positive droplets was generated by Cas12a-mediated non-specific cleavage of the FQ-reporter. Therefore, we first investigated the signal-to-noise (S/N) ratio of the assay at different concentrations of the FQ-reporter. The end-point fluorescence images of the assay at different FQ reporter concentrations (ranging from 250 nM to 2000 nM) are shown in Fig. 3A. The S/N ratio of the assay increased progressively as the concentration of FQ-reporter increased, facilitating

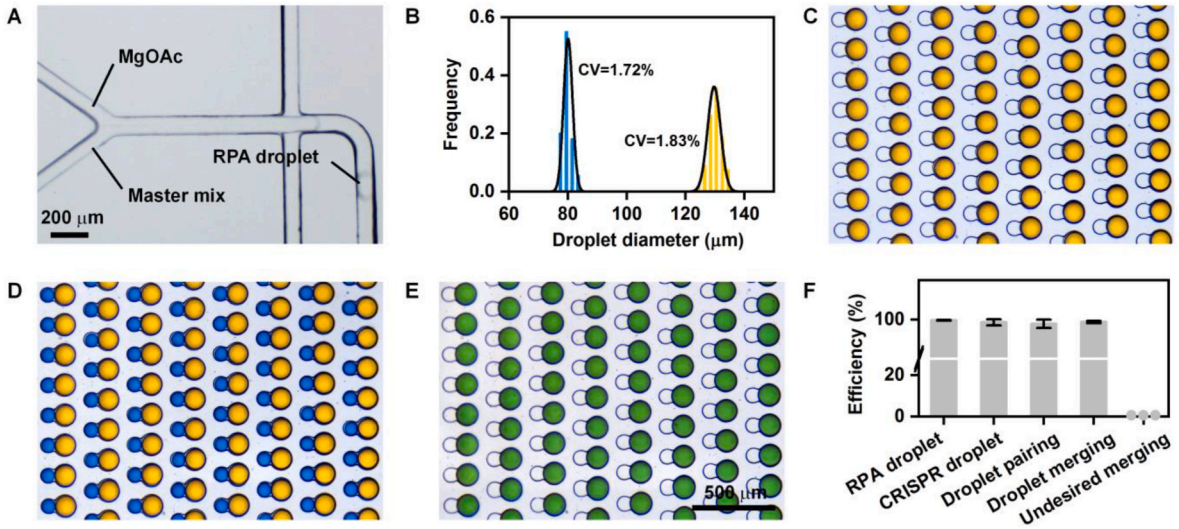


Fig. 2. Characterization of the droplet generation, paring, and merging process. A) The droplet generator with a Y-shaped microchannel for producing the RPA droplets; B) Diameter distribution of the large- and small-volume droplets; C) Trapping of the large-volume droplets containing yellow food dye; D) Trapping of the small-volume droplets containing blue food dye, thus forming one-to-one droplet pairs; E) Merging of the large- and small-volume droplets generates green droplets; F) Efficiencies for droplet trapping, pairing, and merging. Undesired merging during RPA reaction was not observed. Images in C-E) are raw microphotographs captured using the microscope. (For interpretation of the references to colour in this figure legend, the reader is referred to the Web version of this article.)

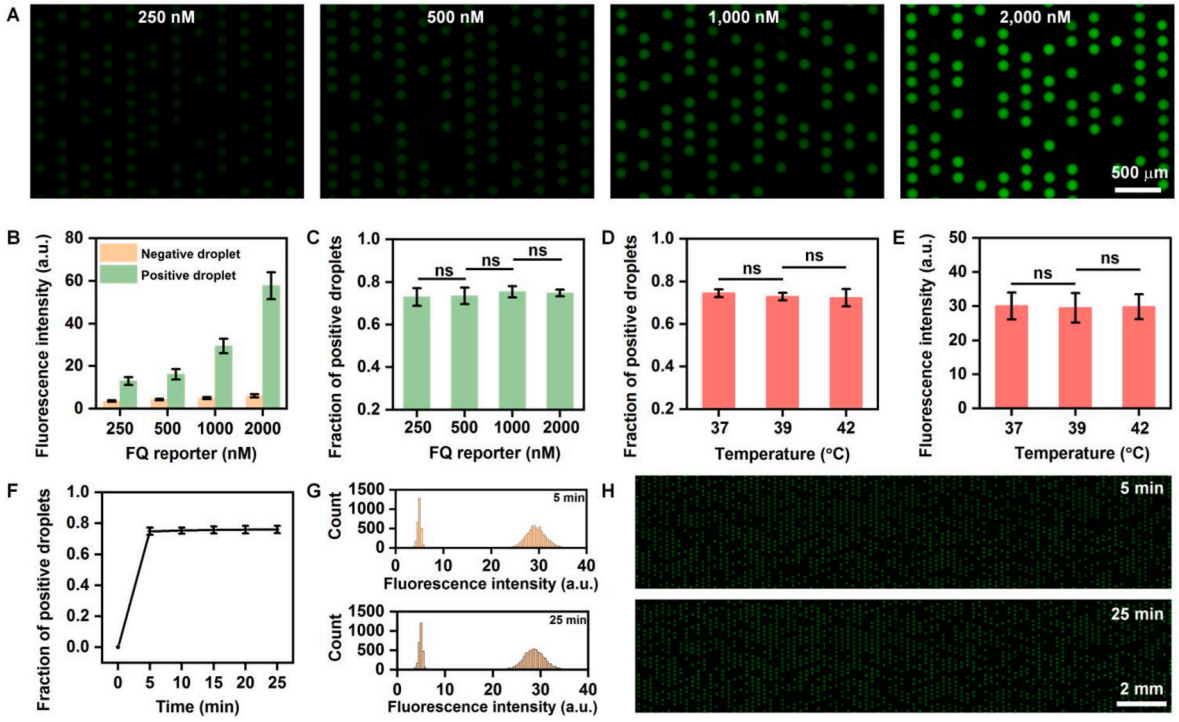


Fig. 3. Optimization of the DIMERIC assay. A) End-point fluorescence images at different FQ-reporter concentrations; B) Mean end-point fluorescence intensity of positive and negative droplets at different FQ-reporter concentrations; C) Fractions of positive droplets at different FQ-reporter concentrations; D) Fractions of positive droplets at different RPA reaction temperatures; E) Mean end-point fluorescence intensity of positive droplets at different RPA reaction temperatures; F) Fractions of positive droplets at different time points for reporter cleavage; G) Fluorescence intensity of all droplets after 5 and 25 min of cleavage; H) End-point fluorescence images of the droplet array after 5 and 25 min of cleavage.

the discrimination between positive and negative droplets (Fig. 3B and Fig. S4). The proportion of positive droplets at different FQ-reporter concentrations was determined by analyzing the fluorescence images. With a constant amount of DNA template, the proportions of positive droplets remained unchanged regardless of the FQ-reporter concentration (Fig. 3C). Considering the S/N ratio (exceeding 5) and assay costs, an FQ-reporter concentration of 1000 nM was selected for the subsequent experiments.

According to the manufacturer's instructions, the optimal reaction temperature for RPA ranges from 37 °C to 42 °C and that for EnGen LbaCas12a ranges from 25 °C to 48 °C. In view of this, we investigated the optimal reaction temperature for the DIMERIC assay. The digital assay was performed at temperatures of 37 °C, 39 °C, and 42 °C to detect the same DNA template. Both the end-point fluorescence intensity

(Fig. 3D) and the proportion (Fig. 3E) of positive droplets resulting from these reactions were found to be comparable. Previous studies have shown that 39 °C or 42 °C was more effective than 37 °C in one-pot digital RPA-CRISPR/Cas12a assays (Wu et al., 2021; Zhang et al., 2023). The different phenomenon observed in our study may be attributed to the following reasons. First, the spatial and temporal separation of the RPA and CRISPR reactions eliminates their mutual interference. Even at suboptimal temperatures, RPA reaction can generate sufficient amplicons to trigger the trans-cleavage activity of Cas12a, which cleaves the majority of the reporters in the droplets. Second, the RPA primers were designed to have lower Tm values and homo-/hetero-primer dimers, resulting in satisfactory amplification efficiency at 37 °C (Table S2). Therefore, a reaction temperature of 37 °C was used in the subsequent experiments.

We next investigated the assay time needed to light-up all the positive droplets. The RPA reaction proceeded for 15 min as previous studies reported (Wang et al., 2019; Zhao et al., 2023), and different Cas12a-mediated cleavage times (5, 10, 15, 20, and 25 min) were tested. As shown in Fig. 3F, the proportion of positive droplets rapidly reached a plateau after 5 min of cleavage and exhibited minimal variation with prolonged incubation. Additionally, the fluorescence intensity distribution of both positive and negative droplets at 5 min and 25 min was similar (Fig. 3G and H), suggesting that a 5-min duration was sufficient for cleaving most of the reporters in the positive droplets. Therefore, all subsequent experiments were performed over a 20-min period, comprising 15 min of RPA reaction followed by 5 min of cleavage.

3.5. The DIMERIC assay for quantitative detection of HBV DNA

After optimizing the reaction conditions, we used a 5-fold serially diluted HBV DNA sample to evaluate the quantification performance of the DIMERIC assay. We emulsified a 50-μL RPA reaction mixture, which contained 10 μL of the DNA sample, into approximately 40,000 1.15-nL droplets (d = 130 μm). This quantity of droplets was sufficient for one sample with three technical replicates. 15 μL of RPA droplet emulsion followed by 5 μL of CRISPR/Cas12a droplet emulsion were successively introduced into the microwell array chip. After the droplets were trapped, excess droplets were flushed out through the outlet of the chip. Taking the number of effective droplets and the volume of the RPA droplet into account, the reaction volume analyzed per chip was approximately 11 μL. The HBV DNA concentration was calculated using Poisson statistics, based on the equation c = -ln(1-k/n)/v. Here, c is the concentration of the target DNA, n is the number of effective droplets determined by droplet trapping, pairing, and merging efficiencies, k is the number of positive droplets counted using imageJ software, and v is the volume of the RPA droplet. As shown in Fig. 4A, the fraction of positive droplets decreased proportionally as the DNA template was diluted, and no false-positive droplets were observed in the no template control (NTC) experiment. The measured DNA concentrations exhibited an excellent linear correlation with the dilution factor (R^2 = 0.99893), demonstrating that this assay was capable of accurately quantifying HBV DNA (Fig. 4B). The quantitative results from the DIMERIC and digital PCR assays exhibited a high degree of concordance, although the values obtained from the DIMERIC assay were marginally lower than those from the digital PCR assay (Fig. 4C). The underestimation of DNA copy numbers can be attributed to the enzyme-mediated nature of DNA melting and primer annealing in RPA, which is susceptible to the interference from hairpin structures, homo-/hetero-primer dimers, secondary structures of DNA templates, and nucleic acid-binding proteins (Shen et al., 2011).

3.6. Quantification of HBV DNA from clinical samples using the DIMERIC assay

Finally, we demonstrated the feasibility of the DIMERIC assay to quantify HBV DNA from clinical serum samples. Twenty-four clinical serum samples were analyzed with qPCR, ddPCR, and the DIMERIC assay, respectively. To detect all HBV variants, the sequences of the genotypes were aligned and the conserved sequences containing PAM sequence (5′-TTTV-3′) were selected for crRNA design (Fig. 5A, B and Table S1). The qPCR amplification curves are shown in Fig. S5 and the end-point fluorescence images of the DIMERIC assay and ddPCR are shown in Fig. 5D and Fig. S6. To ensure comparability, the qPCR results reported in IU/mL (Table S3, clinical outcomes) were converted to copy/mL by multiplying by a conversion factor (1 IU/mL = 5.6 copy/mL according to the manufacturer's instructions). As shown in Fig. 5C, all HBV positive samples (16/24) were consistently detected by qPCR, ddPCR, and the DIMERIC assay, while all negative samples yielded no signals (8/24). Subsequently, we correlated the measured concentrations from the DIMERIC assay with those obtained from qPCR and ddPCR to verify the consistency of their quantitative results. The overall correlations of the measured concentrations from qPCR, ddPCR, and the DIMERIC assay follow the expected trend (Fig. 5E and F). Nevertheless, the correlation between ddPCR and the DIMERIC assay is superior to

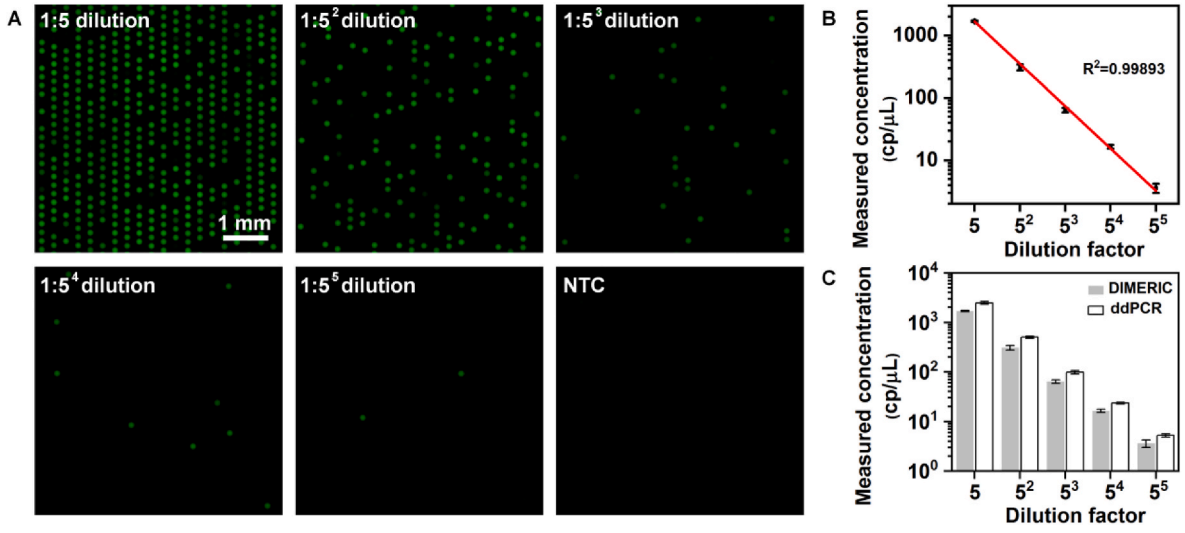


Fig. 4. Quantification performance of the DIMERIC assay. A) Representative end-point fluorescence images of the DIMERIC assay with HBV DNA in a 5-fold dilution series; B) The linear correlation between measured HBV DNA concentrations and the dilution factor (n = 3 technical replicates); C) Measured HBV DNA concentrations by the DIMERIC assay in comparison with a commercial digital PCR instrument (n = 3 technical replicates).

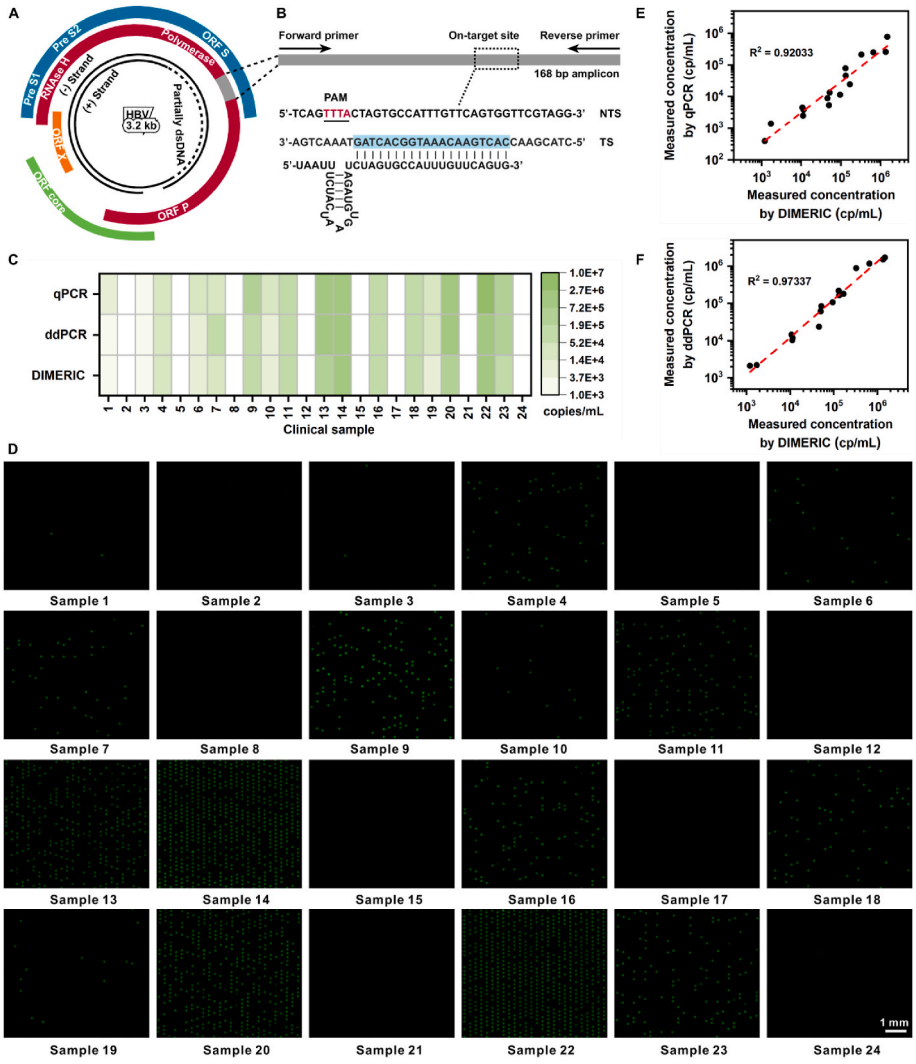


Fig. 5. Clinical validation of the DIMERIC assay. A) HBV genomic map with the target sequence highlighted in gray (on the polymerase coding region); B) Schematic of the target sequence detected by the Cas12a collateral detection. The target site is highlighted in blue and the 5′ PAM sequence is highlighted in red; C) Heat map Illustrating the measured HBV DNA concentrations in 24 clinical serum samples by qPCR, ddPCR, and the DIMERIC assay; D) End-point fluorescence images of the DIMERIC assay for detecting HBV DNA in 24 clinical serum samples; E) Correlation between the HBV DNA concentrations measured by qPCR (clinical outcomes) and the DIMERCI assay. F) Correlation between the HBV DNA concentrations measured by ddPCR and the DIMERIC assay. (For interpretation of the references to colour in this figure legend, the reader is referred to the Web version of this article.)

that between qPCR and the DIMERIC assay ($R^2 = 0.97337$ vs 0.92033). This difference may be attributed to: i) standard curve-based qPCR quantification has high uncertainty compared to ddPCR and the DIMERIC assay; ii) the HBV DNA concentrations in the clinical samples may differ after several freeze-thaw rounds; iii) in-house performed ddPCR and DIMERIC shared the same DNA extracts (Tiangen Biotech.), while qPCR performed in clinical microbiology laboratory used another one (DaAngene).

The DIMERIC assay was compared with the reported digital RPA-CRISPR/Cas12a assays as shown in Table S4 (Wu et al., 2021; Xia et al., 2023; Zhang et al., 2023). In those assays, PAM-free crRNAs located in close proximity to RPA primers were utilized. The ssDNA generated after RPA strand displacement can be recognized by the PAM-free crRNAs, enabling both reactions to proceed concurrently in a droplet. Nevertheless, those assays have several limitations, including location restrictions, unclear optimization mechanisms, and incompatibility with other INA methods (Lin et al., 2023). In contrast, the droplet pairing-merging method can spatially and temporally separate the RPA and CRISPR reactions, thereby resolving the incompatibility between these two reactions. Separating the two reactions not only makes the assay more flexible for design and optimization but also significantly shortens the total assay time. Additionally, the DIMERIC assay has a potential to work with various INA methods, such as LAMP, RCA, and NASBA, along with other Cas enzymes, including Cas9, Cas13, and Cas14.

4. Conclusions

In this study, the DIMERIC assay was developed by deploying a droplet pairing-merging strategy. This assay holds great potential for rapid and precise quantification of pathogenic nucleic acids. First, the removal of reaction incompatibility expedites the accumulation of amplicons, which reduces the time required for both RPA and CRISPR-Cas reactions. Concurrently, the confinement effect of droplets reduces the collateral cleavage time for lightening positive droplets. These combined factors shorten the total assay time of DIMERIC to 20 min. Second, the spatial and temporal separation of RPA and CRISPR reactions eliminates the likelihood of false-negative results. Additionally, incorporating CRISPR detection with digital INA offers enhanced specificity, thereby reducing the probability of false-positive results. Thanks

to these advantages, the DIMERIC assay can provide precise nucleic acid quantification. Future work will be directed towards incorporating optical components and imaging modules to develop a fully integrated device. Additionally, incorporating our previously developed droplet encoding strategy with the DIMERIC assay has the potential to yield a high-order multiplexed digital CRISPR assay. Our method also has substantial potential for reducing sample loss through increasing the number of populated droplets and further optimizing the chip configuration, which can prevent the issues of insufficient detection sensitivity and high measurement uncertainty typically associated with low copy number samples. In conclusion, we are convinced that the DIMERIC assay can serve as a valuable tool for rapid and precise quantification of pathogenic nucleic acids.

CRediT authorship contribution statement

Dongyang Cai: Writing – review & editing, Methodology, Investigation, Funding acquisition, Conceptualization. **Yifan Wang:** Writing – original draft, Methodology, Investigation. **Ziyi Zhang:** Writing – original draft, Methodology, Investigation. **Enqi Huang:** Methodology, Investigation. **Na Yang:** Investigation, Data curation. **Xiao Yang:** Resources. **Ting Zhang:** Resources. **Hongting Wen:** Investigation. **Yu Wang:** Investigation. **Zhenhua Chen:** Writing – review & editing. **Hongkai Wu:** Writing – review & editing. **Dayu Liu:** Writing – review & editing, Supervision, Funding acquisition, Conceptualization.

Declaration of competing interest

The authors declare that they have no known competing financial interests or personal relationships that could have appeared to influence the work reported in this paper.

Acknowledgements

This study was supported by the National Natural Science Foundation of China (82472372, 82202582, 82372345, 82102510); the Natural Science Foundation of Guangdong Province (2024A1515011810); the Guangzhou Key Laboratory of Molecular Imaging and Clinical Translational Medicine (202201020376); and the Science and Technology Projects in Guangzhou (202201010318, 2023A03J0970).

Appendix A. Supplementary data

Supplementary data to this article can be found online at https://doi.org/10.1016/j.bios.2025.117256.

Data availability

Data will be made available on request.

References

Ackerman, C.M., Myhrvold, C., Thakku, S.G., Freije, C.A., Metsky, H.C., Yang, D.K., Ye, S. H., Boehm, C.K., Kosoko-Thoroddsen, T.F., Kehe, J., Nguyen, T.G., Carter, A., Kulesa, A., Barnes, J.R., Dugan, V.G., Hung, D.T., Blainey, P.C., Sabeti, P.C., 2020. Nature 582 (7811), 277–282.

Arizti-Sanz, J., Freije, C.A., Stanton, A.C., Petros, B.A., Boehm, C.K., Siddiqui, S., Shaw, B.M., Adams, G., Kosoko-Thoroddsen, T.F., Kemball, M.E., Uwanibe, J.N., Ajogbasile, F.V., Eromon, P.E., Gross, R., Wronka, L., Caviness, K., Hensley, L.E., Bergman, N.H., MacInnis, B.L., Happi, C.T., Lemieux, J.E., Sabeti, P.C., Myhrvold, C., 2020. Nat. Commun. 11 (1), 5921.

Barrangou, R., Fremaux, C., Deveau, H., Richards, M., Boyaval, P., Moineau, S., Romero, D.A., Horvath, P., 2007. Science 315 (5819), 1709–1712.

Cai, D., Wang, Y., Zou, J., Li, Z., Huang, E., Ouyang, X., Que, Z., Luo, Y., Chen, Z., Jiang, Y., Zhang, G., Wu, H., Liu, D., 2023. Adv. Sci. 10 (7), e2205863.

Chen, B., Gilbert, L.A., Cimini, B.A., Schnitzbauer, J., Zhang, W., Li, G.W., Park, J., Blackburn, E.H., Weissman, J.S., Qi, L.S., Huang, B., 2013. Cell 155 (7), 1479–1491.

Chen, J.S., Ma, E., Harrington, L.B., Da Costa, M., Tian, X., Palefsky, J.M., Doudna, J.A., 2018. Science 360 (6387), 436–439.

Chen, Y., Xu, X., Wang, J., Zhang, Y., Zeng, W., Liu, Y., Zhang, X., 2022. Anal. Chem. 94 (27), 9724–9731.

Choi, J.W., Seo, W.H., Kang, T., Kang, T., Chung, B.G., 2023. Lab Chip 23 (10), 2389–2398.

Cong, L., Ran, F.A., Cox, D., Lin, S., Barretto, R., Habib, N., Hsu, P.D., Wu, X., Jiang, W., Marraffini, L.A., Zhang, F., 2013. Science 339 (6121), 819–823.

Cui, J.Q., Liu, F.X., Park, H., Chan, K.W., Leung, T., Tang, B.Z., Yao, S., 2022. Biosens. Bioelectron. 202, 114019.

Ding, X., Yin, K., Li, Z., Lalla, R.V., Ballesteros, E., Sfeir, M.M., Liu, C., 2020. Nat. Commun. 11 (1), 4711.

Ding, X., Yin, K., Li, Z., Sfeir, M.M., Liu, C., 2021. Biosens. Bioelectron. 184, 113218.

Enqi Huang, Y.W., Cai, Dongyang, Liu, Dayu, 2024. Interdiscip. Médica Sur 2 (1), e20230026.

Gootenberg, J.S., Abudayyeh, O.O., Kellner, M.J., Joung, J., Collins, J.J., Zhang, F., 2018. Science 360 (6387), 439–444.

Gootenberg, J.S., Abudayyeh, O.O., Lee, J.W., Essletzbichler, P., Dy, A.J., Joung, J., Verdine, V., Donghia, N., Daringer, N.M., Freije, C.A., Myhrvold, C., Bhattacharyya, R.P., Livny, J., Regev, A., Koonin, E.V., Hung, D.T., Sabeti, P.C., Collins, J.J., Zhang, F., 2017. Science 356 (6336), 438–442.

Hu, F., Liu, Y., Zhao, S., Zhang, Z., Li, X., Peng, N., Jiang, Z., 2022a. Biosens. Bioelectron. 202, 113994.

Hu, M., Qiu, Z., Bi, Z., Tian, T., Jiang, Y., Zhou, X., 2022b. Proc. Natl. Acad. Sci. U. S. A 119 (26), e2202034119.

Joung, J., Ladha, A., Saito, M., Kim, N.G., Woolley, A.E., Segel, M., Barretto, R.P.J., Ranu, A., Macrae, R.K., Faure, G., Ioannidi, E.I., Krajeski, R.N., Bruneau, R., Huang, M.W., Yu, X.G., Li, J.Z., Walker, B.D., Hung, D.T., Greninger, A.L., Jerome, K. R., Gootenberg, J.S., Abudayyeh, O.O., Zhang, F., 2020. N. Engl. J. Med. 383 (15), 1492–1494.

Kaminski, M.M., Abudayyeh, O.O., Gootenberg, J.S., Zhang, F., Collins, J.J., 2021. Nat. Biomed. Eng. 5 (7), 643–656.

Kulesa, A., Kehe, J., Hurtado, J.E., Tawde, P., Blainey, P.C., 2018. Proc. Natl. Acad. Sci. U. S. A 115 (26), 6685–6690.

Li, L., Li, S., Wu, N., Wu, J., Wang, G., Zhao, G., Wang, J., 2019. ACS Synth. Biol. 8 (10), 2228–2237.

Lin, C., Chen, F., Huang, D., Li, W., He, C., Tang, Y., Li, X., Liu, C., Han, L., Yang, Y., Zhu, Y., Chen, R., Shi, Y., Xia, C., Yan, Z., Du, H., Huang, L., 2023. Biosens. Bioelectron. 239, 115609.

Lin, M., Yue, H., Tian, T., Xiong, E., Zhu, D., Jiang, Y., Zhou, X., 2022. Anal. Chem. 94 (23), 8277–8284.

Liu, F.X., Cui, J.Q., Park, H., Chan, K.W., Leung, T., Tang, B.Z., Yao, S., 2022. Anal. Chem. 94 (15), 5883–5892.

Lu, S., Tong, X., Han, Y., Zhang, K., Zhang, Y., Chen, Q., Duan, J., Lei, X., Huang, M., Qiu, Y., Zhang, D.Y., Zhou, X., Zhang, Y., Yin, H., 2022. Nat. Biomed. Eng. 6 (3), 286–297.

Marraffini, L.A., Sontheimer, E.J., 2008. Science 322 (5909), 1843–1845.

Park, J.S., Hsieh, K., Chen, L., Kaushik, A., Trick, A.Y., Wang, T.H., 2021. Adv. Sci. 8 (5), 2003564.

Shen, F., Davydova, E.K., Du, W., Kreutz, J.E., Piepenburg, O., Ismagilov, R.F., 2011. Anal. Chem. 83 (9), 3533–3540.

Sheth, R.U., Yim, S.S., Wu, F.L., Wang, H.H., 2017. Science 358 (6369), 1457–1461.

Thakku, S.G., Ackerman, C.M., Myhrvold, C., Bhattacharyya, R.P., Livny, J., Ma, P., Gomez, G.I., Sabeti, P.C., Blainey, P.C., Hung, D.T., 2022. PNAS Nexus 1 (1), pgac021.

Uno, N., Li, Z., Avery, L., Sfeir, M.M., Liu, C., 2023. Anal. Chim. Acta 1262, 341258.

Wang, B., Wang, R., Wang, D., Wu, J., Li, J., Wang, J., Liu, H., Wang, Y., 2019. Anal. Chem. 91 (19), 12156–12161.

Wu, H., Cao, X., Meng, Y., Richards, D., Wu, J., Ye, Z., deMello, A.J., 2022. Biosens. Bioelectron. 211, 114377.

Wu, K., Fang, Q., Zhao, Z., Li, Z., 2023. Anal. Chem. 95 (11), 5069–5078.

Wu, X., Tay, J.K., Goh, C.K., Chan, C., Lee, Y.H., Springs, S.L., Wang, Y., Loh, K.S., Lu, T. K., Yu, H., 2021. Biomaterials 274, 120876.

Xia, L., Yin, J., Zhuang, J., Yin, W., Zou, Z., Mu, Y., 2023. Anal. Chem. 95 (10), 4744–4752.

Yao, Z., He, K., Wang, H., Feng, S., Ding, X., Xu, Y., Wang, Q., Xu, X., Wu, Q., Wang, L., 2024. ACS Sens. 9 (7), 3511–3519.

Yeh, E.C., Fu, C.C., Hu, L., Thakur, R., Feng, J., Lee, L.P., 2017. Sci. Adv. 3 (3), e1501645.

Yin, K., Ding, X., Li, Z., Zhao, H., Cooper, K., Liu, C., 2020. Anal. Chem. 92 (12), 8561–8568.

Zhang, C., Cai, Z., Zhou, Z., Li, M., Hong, W., Zhou, W., Yu, D., Wei, P., He, J., Wang, Y., Huang, C., Wang, X., Wu, J., 2023. Biosens. Bioelectron. 222, 114956.

Zhao, F., Hu, Y., Fan, Z., Huang, B., Wei, L., Xie, Y., Huang, Y., Mei, S., Wang, L., Wang, L., Ai, B., Fang, J., Liang, C., Xu, F., Tan, W., Guo, F., 2023. Cell Rep Methods 3 (10), 100620.